Vietnam Journal of Science and Technology ***64***(2) (2026) 305–316
DOI: https://doi.org/10.15625/2525-2518/18545

Synthesis of low-dimensional organo-metal halide perovskite materials

Do Dinh Khai[1], Tran Phuong Mai[1], Vu Thi Minh Hau[1], Phan Vu Thi Van[2], Tran Thi Kim Chi[3], Truong Thanh Tu[1,*], Nguyen-Tran Thuat[2,*]

[1]*Faculty of Chemistry, VNU University of Science, Vietnam National University, 19 Le Thanh Tong, Cua Nam ward, Ha Noi, Viet Nam*
[2]*Nano and Energy Center, VNU University of Science, Vietnam National University 334 Nguyen Trai, Thanh Xuan ward, Ha Noi, Viet Nam*
[3]*Institute of Materials Science, Vietnam Academy of Science and Technology, 18 Hoang Quoc Viet, Nghia Do ward, Ha Noi, Viet Nam*

[*]Emails: *ttruong@hus.edu.vn; thuatnt@vnu.edu.vn*

Received: 18 July 2023; Accepted for publication: 31 December 2023

Abstract. Recently, hybrid organo-metal halide perovskites have rocked the scientific community when going low-dimensional structures. By either simply replacing the organic cation commonly used in three-dimensional materials with a larger one or varying the molar ratio in synthesis reaction, low-dimensional perovskite materials are obtained. In this study, we choose the option of wet chemical synthesis and of mixing precursors in solid state to obtain perovskite crystals with different dimensionality, from zero-dimensional to two-dimensional. Characterization by X-ray diffraction shows that the dimensional characteristic of the material is the one of metal halide octahedra. The zero-dimensional material, formamidinium lead bromide, exhibits a mixture of phase. One-dimensional materials are obtained with unconventional precursors ratio of 1:1 and 2:1, instead of 3:1. Two-dimensional guanidinium lead iodide possesses unprecedented clear diffraction peaks. The photoluminescence results show that these materials have good emission, possessing a wide spectrum, except for one one-dimensional (acetamidinium lead iodide) and one two-dimensional (phenethylamine lead iodide) materials. The intense photoluminescence at room temperature and precise synthesis processes are mandatory results that allow us to go further into a particular optical application of these low-dimensional materials.

Keywords: organo-metal halide perovskite, low dimensional, 0D, 1D, 2D, photoluminescence, exciton.

Classification numbers: 2.1.3, 2.3.1, 2.4.1.

1. INTRODUCTION

Three-dimensional (3D) organo-metal halide perovskite-structured materials, ABX_3, are formed by reacting an equimolar ratio between two precursors, organic salts AX and metal salts BX_2. These amazing materials have astounded the research world with its fascinating quantum and optoelectronic properties [1-5]. One of the wonders is that organic cations can be changed with a large number of choices in the zoology of monovalent, and even multivalent, organic cations [6]. Next by varying the ratio of the initial precursors of the synthesis reaction, the

perovskite crystal is altered and produces what we call a low-dimensional material [7]. In a conventional way, by simply putting precursors into the synthesis reaction, if the ratio between AX and BX_2 is 1:1, a 3D material is obtained. Then at a ratio of 2:1, a two-dimensional (2D) material is synthesized [8]. At 3:1 (or at a ratio of 1:1 but by using a large cation), a one-dimensional (1D) material is obtained [9]. Finally, at 4:1 a zero-dimensional (0D) material is produced [10]. But a low-dimensional perovskite material can be obtained in an unconventional way without obeying the mixture ratio, depending on the size of the organic cation.

The dimensionality of a perovskite material is the dimensionality of the metal halide octahedra, or the way in which they are surrounded by organic cations. The 3D is the case where these octahedra encage organic cations. In the contrary, the 2D is where an octahedral layer is sandwiched by two layers of organic cations. The 1D is where octahedral chains are surrounded by organic cations. And finally, 0D is where each individual octahedron is wrapped by organic cations. The arrangement for 2D, 1D and 0D is a self-assembled process at the molecular level when synthesizing materials. Therefore, we can consider this low-dimensional property to be the nature of the material, which comes from the self-assembling of basic molecules or atoms of a crystal [11-13].

One advantage when using low-dimensional materials in opto-electronic devices is that the combination with a 3D perovskite material exhibits better stability and performance [14-17]. In the case of 1D and 2D materials, the fact that exciton stays in octahedral metal halide layers (for 2D) or lines (for 1D) leads to a higher binding energy, thus opening the possibility of using these 2D and 1D materials for quantum devices at room temperature [18, 19]. In the case of 0D materials, a smallest quantum dot, which is a single lead halide octahedron, is obtained, suggesting a brighter future for optical applications of quantum dot [20].

It is most obvious that the more we investigate the properties of these low-dimensional materials, the higher the urge to find and study further different types of cations that make up different ones. Therefore, constant efforts in finding organic cations with new properties are the driving force for the research presented in this paper. For lead bromide perovskites, the 3D, 2D and 1D formamidinium lead bromide (FAPB) have been thoroughly reported [21, 22], therefore we focus our effort to study the last candidate, which is 0D-FAPB. For lead iodide perovskites, it is true that the zoology of organic cations with our previous study [23-28] leads us to extend to different choices such as 1,4-benzene diammonium, acetamidinium, guanidinium and phenethylamine. In complementarity of find out the synthesis conditions, we try to investigate quickly different optical and structural properties in order to identify the most potential candidate in future quantum and optoelectronic applications.

2. MATERIALS AND METHODS

2.1. Materials and synthesis

Preparation of 0D 0D-FAPB: A mixture of $PbBr_2$ and $CH(NH_2)_2Br$ with a molar ratio of 1:4 was dissolved in dimethylformamide (DMF). $[C(NH_2)_2]_4PbBr_6$ (FA_4PbBr_6 or FAPB) crystals were formed on a glass substrate by a drop-casting method where droplets of precursors were put on the glass surface and let evaporating solvent.

Preparation of 1D 1,4-benzene diammonium lead iodide (1D-BDAPI): A mixture of lead (II) iodide (PbI_2, from Acros) and *1,4*-benzene diammonium iodide ($C_6H_4(NH_3)_2I_2$ – BDAI, from Greatcell) with molar ratio of 1:1 was dissolved in a dilute hydroiodic acid (HI, from Acros) then

the solution was heated to 80-90 °C and stirred for 2 h. Rod-shaped crystals formed during the cooling process of solution were collected, washed with diethyl ether (from Fisher) and dried in vacuum.

Preparation of 1D acetamidinium lead iodide (1D-AAPI): A mixture of acetamidinium iodide ($C_2H_3(NH_2)_2I$ – AAI) and PbI_2 was dissolved in gamma-butyrolactone (GBL) at 90 °C with a molar ratio of 2:1 to prepare acetamidinium lead iodide AA_2PbI_4. The precipitated product was filtered at a hot temperature, then rinsed by acetone for obtaining cleaned yellowish crystals.

*Preparation of 2D guanidinium lead iodide (2D-GAPI): G*uanidinium iodide ($C(NH_2)_3I$ – GAI) and PbI_2 were mixed together in a molar ratio of 2:1 in HI and hypophosphorous acid (H_3PO_2, from Acros) to prepare 2D guanidinium lead iodide GA_2PbI_4. The mixture was heated for 30 min at 65 °C. Then, the solution was slowly cooled to room temperature. After that, the mixture was kept in an icebox for 15 h. Finally, the orange crystals were filtered and collected.

Preparation of 2D phenethylamine lead iodide (2D-PEAPI): $C_6H_5C_2H_4NH_3I$ (PEAI) and PbI_2 were dissolved with 2:1 molar ratio in GBL at 105 °C under stirring for 24 h to form the $(PEA)_2PbI_4$ solution (PEAPI). The solution was slowly reduced to the room temperature (about 30 °C) to generate orange crystals at the bottom of the reaction vessel.

2.2. Characterization

The morphological characterization of all crystals was performed on a SEM Jeol JMS 6490 system, and on a conventional optical microscope. Structural characterization was studied on a D8 ADVANCE- Bruker diffractometer using Cu-Kα radiation with a wavelength λ = 1.5406 Å. For laser-based steady-state photoluminescence (PL) measurements, 355-nm light from a frequency-doubled Nd:YVO_4 laser (700-ps pulse duration, 7-kHz repetition rate) was used as the excitation source to directly excite the perovskite samples. The PL signals were dispersed by using a 0.55-m grating monochromator (Horiba iHR550) and then detected by a thermoelectrically cooled Si-CCD camera (Synapse).

3. RESULTS AND DISCUSSION

3.1. 0D material

Figure 1 illustrates a SEM micrograph of obtained FA_4PbBr_6 crystals. We can observe these crystals as box-shaped with a width about 50 µm and a length between 200 and 300 µm. The crystal face is relatively flat with clear sharp edges.

X-ray diffraction (XRD) pattern of FA_4PbBr_6 material is shown in Figure 2 with diffraction angle ranging from 5 to 70°. When displayed on a logarithmic scale, the diffraction peaks appear quite clearly and sharply. This sharp peak and small width prove that the quality of synthesized FA_4PbBr_6 crystals is quite good. Since this material has just been synthesized and there is only one report on the crystalline structure of FA_4PbBr_6, which is (R3c, $a = b = 13.07$ Å, $c = 18.45$ Å) [29], no further information about the unit cell is available. By using this information, the obtained peaks do not completely coincide with the diffraction pattern of Figure 2. This deviation can be caused by two reasons: (i) our FA_4PbBr_6 material may be a multiphasic/polymorphous material, or (ii) it is necessary to identify the correct crystalline structure by solving single-crystal XRD measurement in future study. We also further examined the crystal properties with a similar material $FA_4PbBr_6.2H_2O$ (P21/n, a =10.3937 Å ,b = 11.3055 Å, c = 10.5519 Å, β = 91.2981°)

[30], however the analysis showed that the peaks position was not quite in agreement. The most special point is the peak at 6.9°, corresponding to the interplanar distance d = 12.6 Å. By comparing with 2D formamidinium lead bromide FA_2PbBr_4 (triclinic P-1, a = 8.5642 Å , b = 11.8840 Å, c = 14.3120 Å, α = 65.9200°, β = 73.0100°, γ = 83.7600°) [22], (001) (002) and to (006) peaks are identified. From this point, we suggest that the FA_4PbBr_6 crystal structure obtained in this study would be likely a mixed phase between the FA_4PbBr_6 and FA_2PbBr_4.

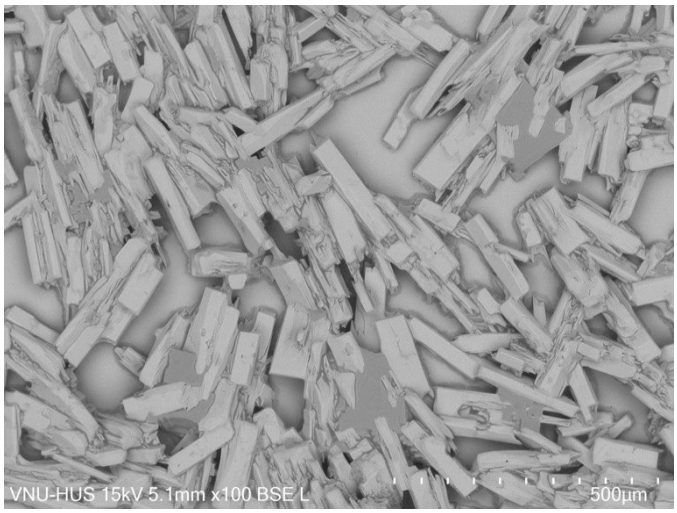

Figure 1. SEM micrograph of 0D FA_4PbBr_6 crystals.

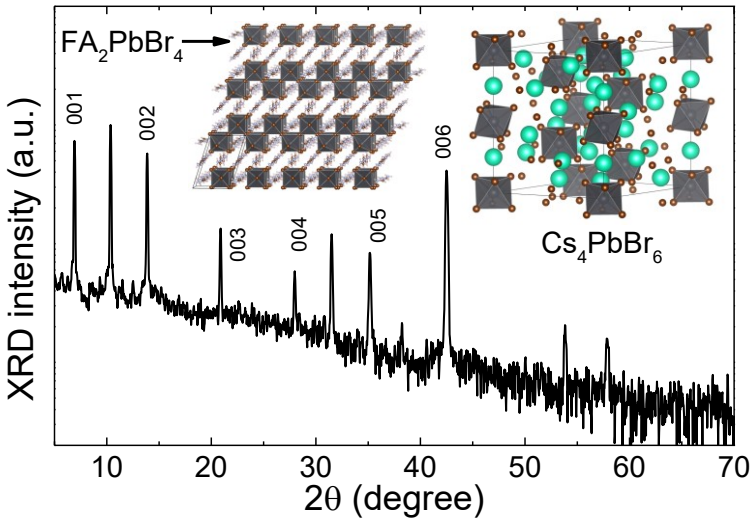

Figure 2. XRD pattern of FA_4PbBr_6 with an inserted similar crystalline structure of Cs_4PbBr_6 (green atoms are Cs, brown ones are Br, and at the core of octahedra are Pb) and with FA_2PbBr_4. Identified peaks are of FA_2PbBr_4.

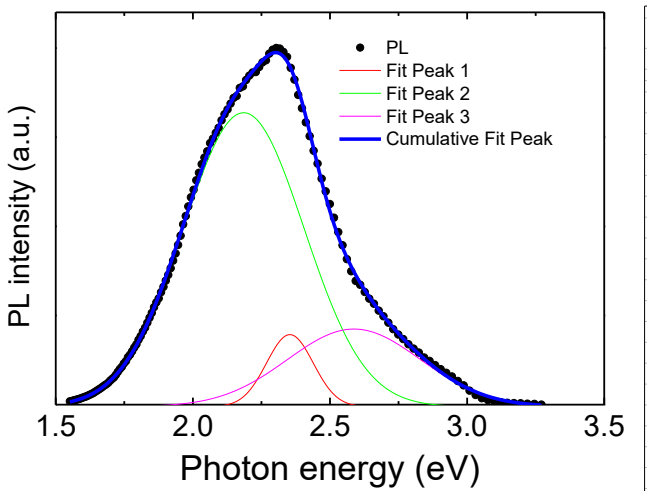

Figure 3. PL spectrum of FA_4PbBr_6.

Figure 3 illustrates a PL spectrum of FA_4PbBr_6 material when excited with a laser with a wavelength of 355 nm. By using a three-Gaussian-peak fitting procedure, we obtain the 2.35 eV peak with a very narrow full width at half maximum (FWHM) of 0.02 eV, while the ones at 2.58 eV and at 2.19 eV have much larger FWHMs, at about 0.52 and 0.57 eV, respectively (see Table 1). We assume that the peak at 2.35 eV corresponds to the emission of an exciton existing in a dot whose size is exactly that of a lead bromide octahedron, which is quite similar to the PL wavelength of Cs_2PbBr_4 nanocrystals [31]. The PL peak at 2.19 eV would much likely correspond to crystal defects or to the exciton self-trapping effect [32].

3.2. 1D material

Figure 4(a) and Figure 4(b show optical microscope images of 1D-BDAPI crystals and 1D-AAPI crystals obtained in this study, respectively. On the microscope images we can clearly see the rod-shaped 1D-BDAPI crystals, with a length of about 200 µm or longer and a width of as small as about 20 µm. With the 1D-AAPI crystals, the morphology is very similar to that of the 1D-BDAPI material.

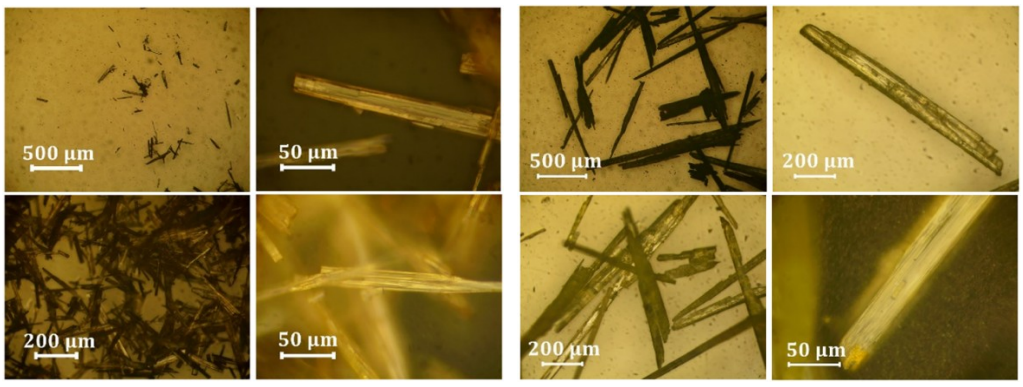

(a) (b)

Figure 4. Optical microscope images of (a) 1D-BDAPI and (b) 1D-AAPI.

Figure 5(a) and Figure 5(b) show the XRD patterns of 1D-BDAPI and 1D-AAPI crystals, respectively, and the inserted figures show the corresponding crystalline structures of these two materials. First, in Figure 5(a), we can see the crystalline structure of long chains composed of octahedra made of lead iodide. Around these chains are arranged organic cations $BDAPI^{2+}$. From the information of a unit cell of 1D-BDAPI, we can clearly determine the reflection family of each XRD peak. Miller indices corresponding to high intensity peaks are shown, for example (110), (020), (200), (220), (230), etc., even with Miller indices as high as (150) and more. This 1D-BDAPI crystal belongs to the Pnnm orthorhombic system with lattice parameters a = 12.952 Å, b = 14.489 Å, c = 4.5851 Å [33]. For 1D-AAPI, there is very little information about the crystalline structure. Nevertheless, XRD peaks of 1D-AAPI is in surprisingly good agreement (up to (710) reflection family) with those of imidazolium lead iodide ($C_3N_2H_5PbI_3$) [34, 35], with following information: group space P63/m of the hexagonal system, lattice parameters $a = b$ = 15.6201 Å and c = 7.9877 Å. In the inserted figure, the crystalline structure of imidazolium lead iodide is exhibited. We can see that this 1D material has face-sharing octahedral chains. It implies therefore that the crystalline structure of 1D-AAPI, once successfully characterized, would be much similar to imidazolium lead iodide.

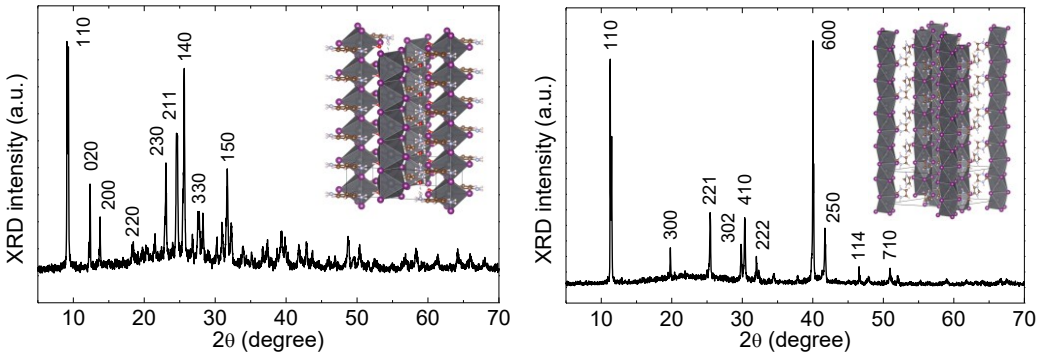

(a) (b)

Figure 5. XRD patterns and inserted 1D crystalline structures of (a) 1D-BDAPI and (b) 1D-AAPI (purple atoms are I, Pb atoms are in the core of octahedra, and the remaining atoms are organic cations). The 1D characteristics is that lead iodide octahedra (edge-sharing for 1D-BDAPI and face-sharing for 1D-AAPI) chains are surrounded by organic cations.

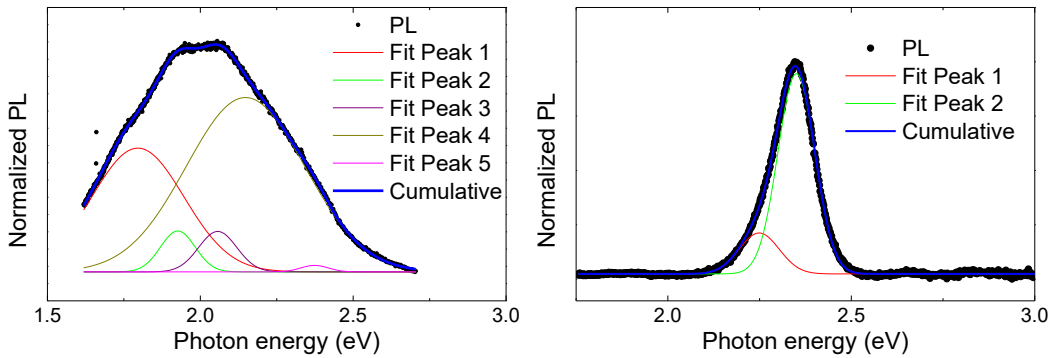

(a) (b)

Figure 6. PL spectra of (a)1D-BDAPI and (b) 1D-AAPI. Broaden PL peaks suggest their self-trapped excitonic nature or from surface/crystal defects.

Figure 6(a) and Figure 6(b) show the emission spectra of 1D-BDAPI and 1D-AAPI crystals, respectively. At first glance, the PL wavelength ranges of these two materials are quite different, the 1D-BDAPI with a broaden emission whereas 1D-AAPI with a narrow one. When performing fitting of PL spectra of these two materials, a number of 2 to 5 Gaussian peaks needs to be used in order to obtain a good agreement between the experiment and the calculation. With 5 Gaussian peaks, the 1D-BDAPI material has emission peaks scattered from 1.97 eV to 2.37 eV (see Table 1). Particularly, the peak at 1.97 eV has the largest FWHM, about 355 meV, while the remaining peaks have FWHM between 100 meV and 150 meV. For the 1D-AAPI material, 2 peaks were obtained with values at 2.249 eV and at 2.350 eV. The FWHM values of these two peaks are quite narrow, at 128 meV and 119 meV, respectively (see Table 1), which is quite similar to the PL peak of bromide perovskites [23, 25, 28]. We assume that these emission peaks correspond to the localized exciton and defects in the crystal; or derive from self-trapped excitons [32].

Table 1. Multi Gaussian peak adjustment of PL spectra.

Peak		0D-FAPB	1D-BDAPI	1D-AAPI	2D-GAPI	2D-PEAPI
1	Position (eV)	2.19 ± 0.01	1.79 ± 0.01	2.249 ± 0.003	1.955 ± 0.001	2.300 ± 0.001
	FWHM (eV)	0.52	0.355	0.128	0.391	0.232
2	Position (eV)	2.354 ± 0.002	1.926 ± 0.003	2.350±0.001	2.157 ± 0.005	2.362 ± 0.001
	FWHM (eV)	0.02	0.134	0.119	0.182	0.061
3	Position (eV)	2.58 ± 0.04	2.057 ± 0.004	N/A	2.318 ± 0.002	N/A
	FWHM (eV)	0.57	0.147	N/A	0.193	N/A
4	Position (eV)	N/A	2.15 ± 0.02	N/A	2.532 ± 0.001	N/A
	FWHM (eV)	N/A	0.456	N/A	0.112	N/A
5	Position (eV)	N/A	2.374 ± 0.005	N/A	N/A	N/A
	FWHM (eV)	N/A	0.107	N/A	N/A	N/A

3.3. 2D material

Figure 7(a) and Figure 7(b) show a SEM micrograph of 2D-GAPI crystals and an optical microscope image of 2D-PEAPI crystals, respectively. These 2D-GAPI crystals are quite large in size, ranging from 50 μm to 200 μm, combined with smooth surfaces and sharp edges. This quality of crystal is much better than the ones that we have synthesized by a method of mixing/grinding the precursors in a solid state [27]. The 2D-PEAPI crystals are exceptionally large, possibly up to 500 μm x 500 μm. This large size has allowed us to exfoliate 2D-PEAPI crystals in order to obtain thin films in small enough number of 2D layers for other optical applications of this material.

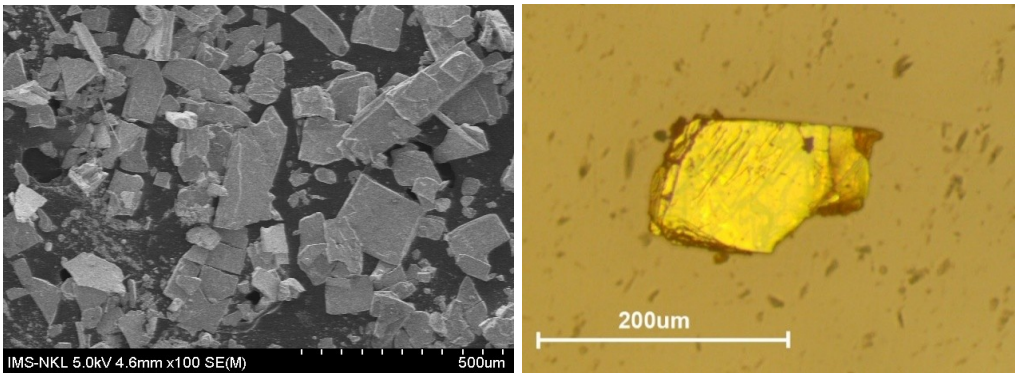

a) b)

Figure 7. SEM micrograph of (a) 2D-GAPI, and optical microscope image of (b) 2D-PEAPI.

Good crystal quality is an important condition for obtaining characteristic diffraction patterns of 2D materials. As a consequence, Figure 8(a) and Figure 8(b) show the XRD patterns of 2D-GAPI and 2D-PEAPI crystals, respectively. A noticeable common property of these two diffraction patterns is that the high intensity peaks appear periodically as a function of the diffraction angle in a periodic manner. This is the most important feature to recognize 2D materials when characterizing with XRD. Indeed, using the single crystal information of 2D-GAPI (orthorhombic system Pmna with a = 12.9291 Å, b = 13.5508 Å, c = 9.3467 Å) [27], the peaks correspond to the reflection families (010), (020), (040), (050), etc. up to (090) are clearly identified. The quality of the 2D-GAPI crystals synthesized in this study is exceptionally good. When looking at the 2D-GAPI crystal structure in Figure 8(c), the following peculiarities can be observed: (i) the 2D planes of lead iodide octahedra is along the (110) orientation of the conventional 3D perovskite [36], and (ii) octahedra layers consist of two staggered ones, and (iii) the 2D layers are stacked in the strongest reflection families or crystalline direction (in Figure 8 it is the Oy direction or 0X0, X = 1, 2, 3 … 9). For 2D-PEAPI material, by using the reported information of the unit cell (triclinic system P1 with a = 8.7389 Å, b = 8.7403 Å, c = 32.9952 Å, $\alpha = 84{,}646$, $\beta = 84{,}657$, $\gamma = 89{,}643$) [37], peaks corresponding to reflection families (002), (004), (006), (008) … up to (0024) are observed. When looking at the crystal structure in Figure 8d, 2D lead iodide octahedral layers can be seen sandwiched between two layers of organic cations PEA^{1+}. These are the special features of the 2D materials synthesized in this report.

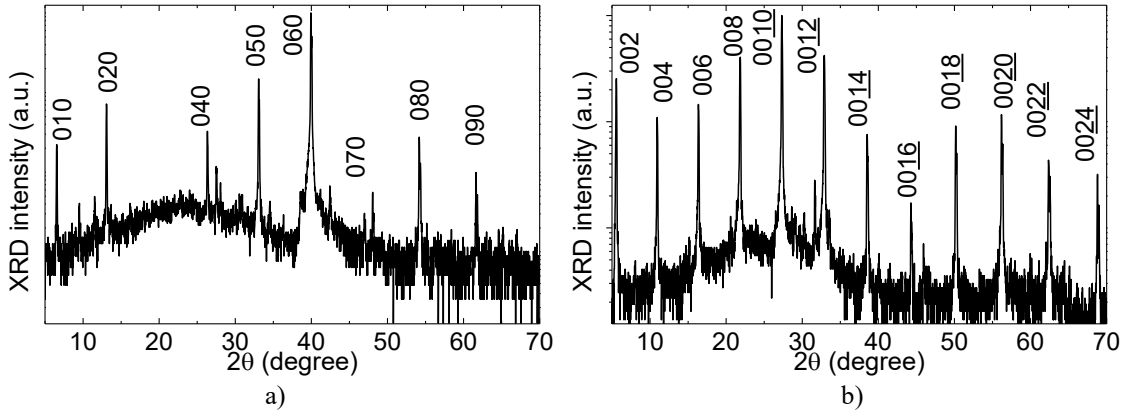

a) b)

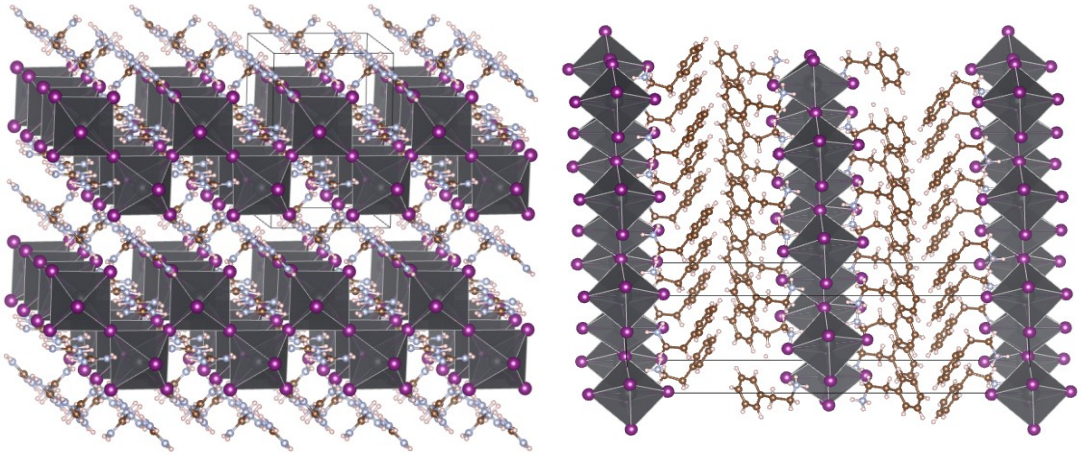

c) d)

Figure 8. XRD pattern of (a) 2D-GAPI (b) 2D-PEAPI and crystalline layered 2D structure of (c) 2D-GAPI (d) 2D-PEAPI (purple atoms are I, Pb atoms are in the core of octahedra, and the remaining atoms are organic cations). The 2D characteristics is that corner-sharing lead iodide octahedra layers are sandwiched by organic cation layers.

The PL spectra of two 2D materials are shown in Figure 9. We can see a clear contrast of the two emission spectra. The 2D-GAPI possesses a spectrum with fairly broaden emission peaks, while that of t he 2D-PEAPI has a narrow one. When adjusting with four Gaussian peaks, the emission spectrum of 2D-GAPI gives three peaks with large FWHM, from about 180 meV to about 390 meV, and one narrow peak at 2.53 eV. This particular peak has a FWHM at 112 meV (see Table 1). For 2D-PEAPI, we can see that the spectrum can be fitted with only two Gaussian peaks. One of these, at 2.362 eV has a very small FWHM, at 61 meV (see Table 1). The small FWHM peak is shown to originate from recombination of free excitons (eg. the 2.362 eV peak for 2D-PEAPI and 2.53 eV for 2D-GAPI) [27]. The remaining peaks with large FWHM are usually derived from self-trapped excitons as other studies have indicated [38].

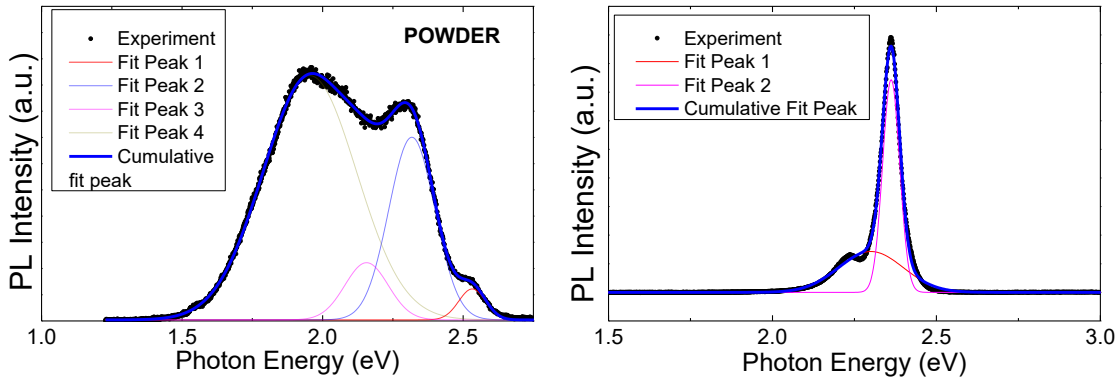

(a) (b)

Figure 9. PL spectra of (a) 2D-GAPI (b) 2D-PEAPI.

4. CONCLUSIONS

To summarize, in this paper we have presented an experimental study on the synthesis of different types of hybrid organo-metal halide perovskite materials with dimensional numbers from zero to two. The dimensionality of these materials correspond to the dimensionality of the lead iodide octahedra. The 0D case corresponds to the case where single octahedra are surrounded by organic cations. For the 2D case, by using a 2:1 molar ratio between the organic salt and the metal one, a 2D material is obtained. The most special case is the 1D one where this ratio is 1:1 and 2:1, however, because the size of the organic cations is large enough, the resulting material is not similar to the traditional 3D or 2D perovskite materials but 1D. Characterization by XRD diffraction shows that the quality of the obtained crystals is quite good. In the case of 2D, repeated periodic peak pattern is observed. When investigated by photoluminescence spectroscopy, most materials give broad peak emission spectrum, except for the cases of 1D-AAPI and 2D-PEAPI materials which possess a very strong and narrow peak. This feature is derived from the recombination of free excitons in crystals. This research serves as a premise to open up other directions of application of this system in optoelectronics and advanced quantum devices.

Acknowledgements. This research is funded by Vietnam National Foundation for Science and Technology Development (NAFOSTED) under grant number 103.02-2019.361.

CRediT authorship contribution statement. Author contributions: Do Dinh Khai: Investigation, Methodology, Writing – original draft. Tran Phuong Mai, Vu Thi Minh Hau, Phan Vu Thi Van: Investigation. Tran Thi Kim Chi: Investigation. Truong Thanh Tu: Methodology, Supervision, Writing – original draft. Nguyen-Tran Thuat: Methodology, Supervision, Funding acquisition, Writing – original draft.

Declaration of competing interest. The authors declare that they have no known competing financial interests or personal relationships that could have appeared to influence the work reported in this paper.

REFERENCES

1. Kim Y. H., Cho H., Lee T. W. - Metal halide perovskite light emitters. Proc. Natl. Acad. Sci., **113**(42) (2016) 11694-11702. https://doi.org/10.1073/pnas.1607471113.
2. Wang H., Kim D. H. - Perovskite-based photodetectors: Materials and devices. Chem. Soc. Rev., **46**(17) (2017) 5204-5236. https://doi.org/10.1039/c6cs00896h.
3. Zuo C., Bolink H. J., Han H., Huang J., Cahen D., Ding L. - Advances in Perovskite Solar Cells. Adv. Sci., **3**(7) (2016) 1500324. https://doi.org/10.1002/advs.201500324.
4. Sutherland B. R., Sargent E. H. - Perovskite photonic sources. Nat. Photonics, **10**(5) (2016) 295-302. https://doi.org/10.1038/nphoton.2016.62.
5. Stranks S. D., Snaith H. J. - Metal-halide perovskites for photovoltaic and light-emitting devices. Nat. Nanotechnol., **10**(5) (2015) 391-402. https://doi.org/10.1038/nnano.2015.90.
6. Mao L., Stoumpos C. C., Kanatzidis M. G. - Two-Dimensional Hybrid Halide Perovskites: Principles and Promises. J. Am. Chem. Soc., **141**(3) (2019) 1171-1190. https://doi.org/10.1021/jacs.8b10851.
7. Saidaminov M. I., Mohammed O. F., Bakr O. M. - Low-Dimensional-Networked Metal Halide Perovskites: The Next Big Thing. ACS Energy Lett., **2**(4) (2017) 889-896. https://doi.org/10.1021/acsenergylett.6b00705.
8. Li X., Hoffman J. M., Kanatzidis M. G. - The 2D halide perovskite rulebook: How the spacer influences everything from the structure to optoelectronic device efficiency. Chem. Rev., **121**(4) (2021) 2230-2291. https://doi.org/10.1021/acs.chemrev.0c01006.

9. Jodlowski A. D., Yépez A., Luque R., Camacho L., de Miguel G. - Benign-by-Design Solventless Mechanochemical Synthesis of Three-, Two-, and One-Dimensional Hybrid Perovskites. Angew. Chem. Int. Ed., **55**(48) (2016) 14972-14977. https://doi.org/10.1002/anie.201607397.
10. Chen Y., Zhou Y., Zhao Q., Zhang J. Y., Ma J., Xuan T., Guo S. Q., Yong Z. J., Wang J., Kuroiwa Y., Moriyoshi C., Sun H. T. - $Cs_4PbBr_6/CsPbBr_3$ Perovskite Composites with Near-Unity Luminescence Quantum Yield: Large-Scale Synthesis, Luminescence and Formation Mechanism, and White Light-Emitting Diode Application. ACS Appl. Mater. Interfaces, **10**(18) (2018) 15905-15912. https://doi.org/10.1021/acsami.8b04556.
11. Stoumpos C. C., Kanatzidis M. G. - Halide Perovskites: Poor Man's High-Performance Semiconductors. Adv. Mater., **28**(28) (2016) 5778-5793. https://doi.org/10.1002/adma.201600265.
12. Blancon J., Stier A. V., Tsai H., Nie W., Stoumpos C. C., Traoré B., Pedesseau L., Kepenekian M., Katsutani F., Noe G. T., Kono J., Tretiak S., Crooker S. A., Katan C., Kanatzidis M. G., Crochet J. J., Even J., Mohite A. D. - Scaling law for excitons in 2D perovskite quantum wells. Nat. Commun., **9**(1) (2018) 2254. https://doi.org/10.1038/s41467-018-04659-x.
13. Zuo C., Scully A. D., Vak D., Tan W., Jiao X., McNeill C. R., Angmo D., Ding L., Gao M. - Self-Assembled 2D Perovskite Layers for Efficient Printable Solar Cells. Adv. Energy Mater., **9**(4) (2019) 1803258. https://doi.org/10.1002/aenm.201803258.
14. Liao Y., Liu H., Zhou W., Yang D., Shang Y., Shi Z., Li B., Jiang X., Zhang L., Quan L. N., Quintero-Bermudez R., Sutherland B. R., Mi Q., Sargent E. H., Ning Z. - Highly Oriented Low-Dimensional Tin Halide Perovskites with Enhanced Stability and Photovoltaic Performance. J. Am. Chem. Soc., **139**(19) (2017) 6693-6699. https://doi.org/10.1021/jacs.7b01815.
15. Mao L., Wu Y., Stoumpos C. C., Wasielewski M. R., Kanatzidis M. G. - White-Light Emission and Structural Distortion in New Corrugated Two-Dimensional Lead Bromide Perovskites. J. Am. Chem. Soc., **139**(14) (2017) 5210-5215. https://doi.org/10.1021/jacs.7b01312.
16. Wang D., Wright M., Elumalai N. K., Uddin A. - Stability of perovskite solar cells. Sol. Energy Mater. Sol. Cells, **147** (2016) 255-275. https://doi.org/10.1016/j.solmat.2015.12.025.
17. Qiu T., Hu Y., Xu F., Yan Z., Bai F., Jia G., Zhang S. - Recent advances in one-dimensional halide perovskites for optoelectronic applications. Nanoscale, **10**(45) (2018) 20963-20989. https://doi.org/10.1039/c8nr05862h.
18. Fieramosca A., Polimeno L., Ardizzone V., De Marco L., Pugliese M., Maiorano V., De Giorgi M., Dominici L., Gigli G., Gerace D., Ballarini D., Sanvitto D. - Two-dimensional hybrid perovskites sustaining strong polariton interactions at room temperature. Sci. Adv., **5**(5) (2019) eaav9967. https://doi.org/10.1126/sciadv.aav9967.
19. Su R., Diederichs C., Wang J., Liew T. C. H., Zhao J., Liu S., Xu W., Chen Z., Xiong Q. - Room-Temperature Polariton Lasing in All-Inorganic Perovskite Nanoplatelets. Nano Lett., **17**(6) (2017) 3982-3988. https://doi.org/10.1021/acs.nanolett.7b01956.
20. Zhang H., Liao Q., Wu Y., Chen J., Gao Q., Fu H. - Pure zero-dimensional Cs_4PbBr_6 single crystal rhombohedral microdisks with high luminescence and stability. Phys. Chem. Chem. Phys., **19**(43) (2017) 29092-29098. https://doi.org/10.1039/C7CP06097A.
21. Minh D. N., Nguyen L. A. T., Trinh C. T., Oh C., Eom S., Vu T. V., Choi J., Sim J. H., Lee K., Kim J., Cho S. C., Lee S. U., Cimrová V., Kang Y. - Low-Dimensional Single-Cation Formamidinium Lead Halide Perovskites ($FA_{m+2}Pb_mBr_{3m+2}$): From Synthesis to Rewritable Phase-Change Memory Film. Adv. Funct. Mater., **31**(17) (2021) 2011093. https://doi.org/10.1002/adfm.202011093.
22. Fateev S. A., Petrov A. A., Marchenko E. I., Zubavichus Y. V., Khrustalev V. N., Petrov A. V., Aksenov S. M., Goodilin E. A., Tarasov A. B. - FA_2PbBr_4: Synthesis, Structure, and Unusual Optical Properties of Two Polymorphs of Formamidinium-Based Layered (110) Hybrid Perovskite. Chem. Mater., **33**(5) (2021) 1900-1907. https://doi.org/10.1021/acs.chemmater.1c00382.
23. Phan Vu T. V., Nguyen M. T., Nguyen D. T. T., Vu T. D., Nguyen D. L., An N. M., Nguyen M. H., Sai C. D., Bui V. D., Hoang C. H., Truong T. T., Lai N. D., Nguyen-Tran T. - Three-Photon Absorption Induced Photoluminescence in Organo-Lead Mixed Halide Perovskites. J. Electron. Mater., **46**(6) (2017) 3622-3626. https://doi.org/10.1007/s11664-017-5407-y.

24. Thuat N. T., An M. N., Luong T. T., Nguyen H. H., Truong T. T. - Growth of single crystals of methylammonium lead mixed-halide perovskites. Commun. Phys., **28**(3) (2018) 237. https://doi.org/10.15625/0868-3166/28/3/12666.
25. Nguyen-Tran T., Truong T. T., Nguyen T. M., Nguyen D. T., Luu Q. M., Nguyen H. H., Tran C. T. K., Bui H. T. T. - Growth and morphology control of $CH_3NH_3PbBr_3$ crystals. J. Mater. Sci., **54**(24) (2019) 14797-14808. https://doi.org/10.1007/s10853-019-03943-5.
26. Nguyen-Tran T., An N. M., Nguyen K. D., Nguyen T. D., Truong T. T. - Synthesis of organo tin halide perovskites via simple aqueous acidic solution-based method. J. Sci.: Adv. Mater. Devices, **3**(4) (2018) 471-477. https://doi.org/10.1016/j.jsamd.2018.08.004.
27. Nguyen-Tran T., Dinh V. A., Van Ly N., Luong H. D., Pham D. T., Truong T. T., Nguyen H. Q., Dao Q. D., Kim Tran C. T., Thu Bui H. T., Nguyen D. T., Ha Dang M. N., Thi Phan V. V., Truong Q. D. - Novel (110) Double-Layered Guanidinium-Lead Iodide Perovskite Material: Crystal Structure, Electronic Structure, and Broad Luminescence. J. Phys. Chem. C, **125**(1) (2021) 964-972. https://doi.org/10.1021/acs.jpcc.0c08540.
28. Nguyen M. T., Phan Vu T. V., Bui B. T., Luong T. T., Nguyen M. H., Hoang Ngoc L. H., Bui V. D., Truong T. T., Nguyen-Tran T. - Optical and Structural Study of Organometal Halide Materials for Applications in Perovskite-Based Solar Cells. J. Electron. Mater., **45**(5) (2016) 2322-2327. https://doi.org/10.1007/s11664-015-4273-8.
29. Nguyen L. A. T., Minh D. N., Yuan Y., Samanta S., Wang L., Zhang D., Hirao N., Kim J., Kang Y. - Pressure-induced fluorescence enhancement of $FA_\alpha PbBr_{2+\alpha}$ composite perovskites. Nanoscale, **11**(13) (2019) 5868-5873. https://doi.org/10.1039/C8NR09780A.
30. Wakamiya A., Endo M., Sasamori T., Tokitoh N., Ogomi Y., Hayase S., Murata Y. - Reproducible fabrication of efficient perovskite-based solar cells: X-ray crystallographic studies on the formation of $CH_3NH_3PbI_3$ layers. Chem. Lett., **43**(5) (2014) 711-713. https://doi.org/10.1246/cl.140074.
31. Zhang Y., Saidaminov M. I., Dursun I., Yang H., Murali B., Alarousu E., Yengel E., Alshankiti B. A., Bakr O. M., Mohammed O. F. - Zero-Dimensional Cs_4PbBr_6 Perovskite Nanocrystals. J. Phys. Chem. Lett., **8**(5) (2017) 961-965. https://doi.org/10.1021/acs.jpclett.7b00105.
32. Hu T., Smith M. D., Dohner E. R., Sher M. J., Wu X., Trinh M. T., Fisher A., Corbett J., Zhu X. Y., Karunadasa H. I., Lindenberg A. M. - Mechanism for Broadband White-Light Emission from Two-Dimensional (110) Hybrid Perovskites. J. Phys. Chem. Lett., **7**(12) (2016) 2258-2263. https://doi.org/10.1021/acs.jpclett.6b00793.
33. Lemmerer A., Billing D. G. - Two packing motifs based upon chains of edge-sharing PbI_6 octahedra. Acta Crystallogr., Sect. C: Cryst. Struct. Commun., **62**(Pt 12) (2006) m597-m601. https://doi.org/10.1107/S0108270106039746.
34. Arora Y., Seth C., Khushalani D. - Crafting Inorganic Materials for Use in Energy Capture and Storage. Langmuir, **35**(28) (2019) 9101-9114. https://doi.org/10.1021/acs.langmuir.8b02953.
35. Seth C., Khushalani D. - Non-Perovskite Hybrid Material, Imidazolium Lead Iodide, with Enhanced Stability. ChemNanoMat, **5**(1) (2019) 85-91. https://doi.org/10.1002/cnma.201800375.
36. Daub M., Haber C., Hillebrecht H. - Synthesis, Crystal Structures, Optical Properties, and Phase Transitions of the Layered Guanidinium-Based Hybrid Perovskites $[C(NH_2)_3]_2MI_4$; M = Sn, Pb. Eur. J. Inorg. Chem., **2017**(7) (2017) 1120-1126. https://doi.org/10.1002/ejic.201601499.
37. Du K., Tu Q., Zhang X., Han Q., Liu J., Zauscher S., Mitzi D. B. - Two-Dimensional Lead(II) Halide-Based Hybrid Perovskites Templated by Acene Alkylamines: Crystal Structures, Optical Properties, and Piezoelectricity. Inorg. Chem., **56**(15) (2017) 9291-9302. https://doi.org/10.1021/acs.inorgchem.7b01094.
38. Mauck C. M., Tisdale W. A. - Excitons in 2D Organic-Inorganic Halide Perovskites. Trends Chem., **1**(4) (2019) 380-393. https://doi.org/10.1016/j.trechm.2019.04.003.